chemistry

MDPI

Article

Photodynamic Action of Synthetic Curcuminoids against *Staphylococcus aureus*: Experimental and Computational Evaluation

Nícolas J. Melo [1], Jennifer M. Soares [1], Lívia N. Dovigo [2], Christian Carmona-Vargas [3], Antônio S. N. Aguiar [4], Adriana C. dos Passos [4], Kleber T. de Oliveira [3], Vanderlei S. Bagnato [1,5], Lucas D. Dias [1,4,*] and Natalia Inada [1,*]

[1] Group of Optics, São Carlos Institute of Physics, University of São Paulo, Av. Trabalhador São-Carlense, 400, São Carlos 13566-590, SP, Brazil; nicolas.junhiti.melo@usp.br (N.J.M.); vander@ifsc.usp.br (V.S.B.)
[2] Department of Social Dentistry, Araraquara Dental School, São Paulo State University, São Paulo 14801-385, SP, Brazil; livia.dovigo@unesp.br
[3] Department of Chemistry, Federal University of São Carlos, São Carlos 13565-905, SP, Brazil; ccamiloc30@gmail.com (C.C.-V.); kleber.oliveira@ufscar.br (K.T.d.O.)
[4] Laboratório de Novos Materiais, Universidade Evangélica de Goiás, Anápolis 75083-515, GO, Brazil; antonio.aguiar@docente.unievangelica.edu.br (A.S.N.A.)
[5] Department of Biomedical Engineering, Texas A&M University, College Station, TX 77843, USA
* Correspondence: lucasdanillodias@gmail.com (L.D.D.); nataliainada@ifsc.usp.br (N.I.)

Abstract: Natural curcumin is composed of three curcuminoids, namely curcumin (CUR), demethoxycurcumin (DMC) and bis-demethoxycurcumin (BDMC). These compounds are utilized in various biophotonics applications, including photodynamic therapy (PDT). This work aimed to evaluate the photodynamic action (alternative to antibiotics) of synthetic curcuminoids against *Staphylococcus aureus*. Herein, we evaluated an optimal proportion of the three curcuminoids mixed in solution to improve photoinactivation effects. Therefore, a set of computational calculations was carried out to understand the photodynamic action (stability and mechanism) of curcuminoids. Regarding computational analysis, the curcuminoid molecules were optimized using DFT with the hybrid exchange–correlation functional M06-2X, which includes long-range correction, and the 6-311++G(d,p) basis set. DMC and BDMC were more effective as photosensitizers than curcumin at a very low concentration of 0.75 μM, inactivating more than five orders of magnitude of *S. aureus*. Theoretical UV-vis absorption spectra showed that at maximum absorption wavelengths, electronic transitions of the $\pi \rightarrow \pi^*$ type originated from H→L excitations. The BDMC was more stable than the other two curcuminoids after photobleaching, and the fluorescence emission was also higher, which could lead to its usage as a fluorescence dye to track bacteria. In fact, the results of electronic structure calculations proved that the stability order of curcuminoids is CUR < DMC < BDMC. The mixture of synthetic curcuminoids was more effective in the inactivation of *S. aureus* compared to curcumin by itself; for all proposed mixtures, an equal or superior reduction was achieved.

Keywords: curcumin; demethoxycurcumin; bis-demethoxycurcumin; curcuminoids; photodynamic inactivation; molecular modeling; *Staphylococcus aureus*

Citation: Melo, N.J.; Soares, J.M.; Dovigo, L.N.; Carmona-Vargas, C.; Aguiar, A.S.N.; dos Passos, A.C.; de Oliveira, K.T.; Bagnato, V.S.; Dias, L.D.; Inada, N. Photodynamic Action of Synthetic Curcuminoids against *Staphylococcus aureus*: Experimental and Computational Evaluation. *Chemistry* **2024**, *6*, 581–600. https://doi.org/10.3390/chemistry6040035

Academic Editor: Felix Plasser

Received: 16 May 2024
Revised: 15 July 2024
Accepted: 22 July 2024
Published: 25 July 2024

1. Introduction

Throughout human history, pathogenic bacteria have loomed large, causing significant mortality and economic burden. The golden age of antibiotics, stretching from the 1930s to the 1960s, saw the discovery of numerous life-saving drugs. These drugs proved invaluable not only in treating civilian illnesses but also in protecting soldiers during World War II [1,2]. However, the discovery of new antibiotics has slowed dramatically, while the number of resistant pathogens continues to rise. This trend of increasing antibiotic resistance is a cause for serious concern, as it threatens to render conventional antibiotic

treatments ineffective once again [3]. The economic impact of antimicrobial resistance is also substantial, costing countries like the United States billions of dollars in healthcare expenses and lost productivity [4]. Furthermore, low- and middle-income countries are likely to bear the brunt of this problem, with increased poverty and lost productivity due to illness and premature death [5].

Considering all the difficulties regarding the discovery and commercialization of new antibiotics, research on alternative antimicrobial techniques has significantly increased. Photodynamic therapy (PDT) has emerged as a promising technique with growing applications in recent years, including treatments for skin cancer and microbial control [6–9]. Its mechanism is based on photon absorption by a photosensitizing molecule with joint interaction of light and molecular oxygen (O_2) to produce reactive oxygen species (ROS) by two types of reactions. In Type 1 reactions, electron transfer to organic substrates occurs, forming ions that interact with O_2 and form hydrogen peroxide (H_2O_2), superoxide radical anion ($O_2^{\cdot-}$), and hydroxyl radical (·OH). In Type 2 reactions, the excited triplet photosensitizer reacts directly with molecular oxygen, exciting it to the singlet oxygen state ($^1O_2$) which interacts with cellular macromolecules such as unsaturated lipids, amino acids, proteins, and nucleic acids, promoting cell death [10–12].

Regarding the quantum mechanical calculations, these studies are an important tool for predicting various physical and chemical properties of molecules. Several quantum mechanical methods are available, such as the Hartree–Fock [13], density functional theory (DFT) [14], and semi-empirical [15] methods. Each of these methods varies in complexity, accuracy, and applicability to different types of systems. The most popular among them is DFT, which is based on the idea that all the fundamental properties of a quantum system with many electrons can be determined from the electron density of the system. DFT is founded on two theorems: the Hohenberg–Kohn theorem [16], which states that the electron density of a system in the ground state uniquely determines the total energy of the system and other properties and that there is a universal density functional that can be used to determine the total energy; and the Kohn–Sham theorem [17], which proposes a series of equations that solve the many-electron problem by transforming it into a set of single-electron problems moving in an effective potential. DFT is used in a wide range of applications in chemistry, physics, and materials science. One of its main uses is in geometry optimization, where the most stable structures of molecules and solids are determined. This is important for understanding the shape and fundamental properties of materials. In the calculation of bond dissociation energy, DFT can determine the energy required to break chemical bonds, providing insights into the stability of molecules and their chemical reactivity. Another important application is in the study of electronic properties, such as band gaps in semiconductor materials, which are essential for the development of electronic and photonic devices [18]. DFT is also widely used to predict spectra in various spectroscopic techniques, including UV-Vis, infrared (IR), and nuclear magnetic resonance (NMR) spectra, allowing the interpretation of experimental data and the identification of molecular structures. Additionally, it can identify transition states and intermediates, which are essential in the analysis of chemical reactions, providing a detailed understanding of reaction mechanisms [18].

Regarding the scope of available photosensitizers, curcumin is one of the remarkable natural photosensitizers, encountered in the rhizomes of *Curcuma longa*, a plant of the Zingiberaceae family [19]. Natural curcumin extract, also known as turmeric (from the *C. longa* rhizome after purification) is composed of three curcuminoids (Figure 1), namely, curcumin (CUR), demethoxycurcumin (DMC), and bis-demethoxycurcumin (BDMC) [20]. Although curcuminoids are naturally present in the rhizome of Curcuma longa in varying amounts [11], their actual content can fluctuate depending on planting conditions and local climate. This variability can make it challenging to achieve consistent results when using natural extracts of turmeric [19,21]. Given the different possible compositions of these natural products, the availability of each curcuminoid obtained by chemical synthesis

would overcome these obstacles, allowing us to understand each curcuminoid's potential as a photosensitizer.

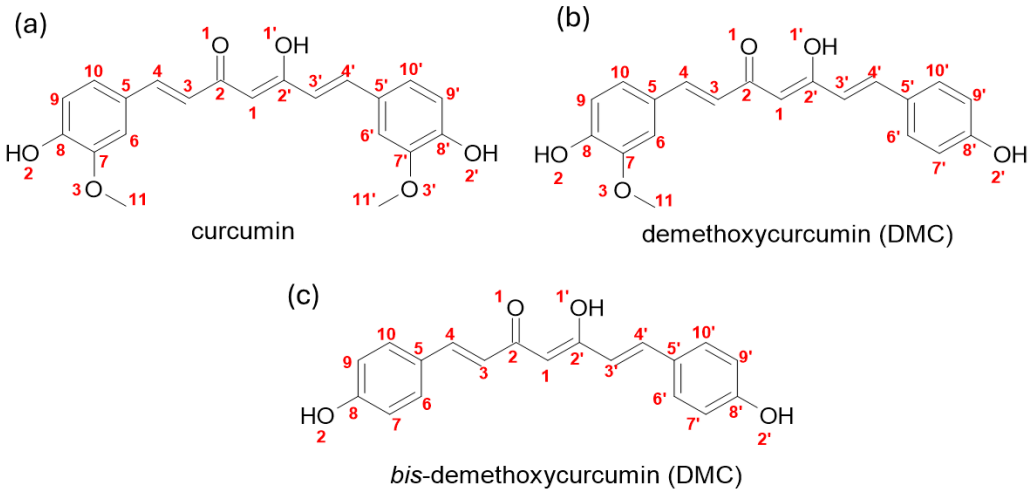

Figure 1. Molecular structure of the three curcuminoids found in *Curcuma longa*: (**a**) Curcumin, (**b**) demethoxycurcumin, (**c**) bis-demethoxycurcumin.

Consequently, the controlled synthesis of curcumin (CUR) and its natural derivatives, demethoxycurcumin (DMC) and bis-demethoxycurcumin (BDMC), has gained significant interest. This approach fosters the reproducibility of protocols in both laboratory settings and, crucially, clinical trials. In clinical settings, the focus lies on optimizing procedures utilizing PDI to ensure effective photodynamic activity in treatment [9,22]. Additionally, by obtaining each curcuminoid it is possible to use each molecule or their different mixtures as photosensitizers.

The use of DMC and BDMC as photosensitizers can be found in some PDT studies, especially for the treatment of tumors [23–26]. However, not much is published regarding its usage in the PDI of microorganisms. Since turmeric is composed of CUR, DMC, and BDMC, this research aimed to study which synthetic pigments had the highest photodynamic activity against *Staphylococcus aureus*. Another objective is to understand whether there is an optimal proportion of the three molecules mixed in solution to improve photoinactivation effects and, alternatively, if synergistic effects can be seen when combining curcuminoids. An investigation on their biophysical characteristics is briefly described using spectrophotometry.

2. Materials and Methods

2.1. Chemicals

DMSO (dimethylsulfoxide) was purchased from Synth, São Paulo, Brazil. *Staphylococcus aureus* (ATCC 25923) was purchased from the American Type Culture Collection (Manassas, VA, USA). Brain Heart Infusion (BHI) medium was purchased from Kasvi (São José dos Pinhais, Paraná, Brazil).

Curcuminoids were synthesized [22] and solubilized in dimethylsulfoxide, (DMSO), for an initial concentration of 4.88 mM. Dilutions were performed with distilled water for work concentrations (Table 1). The curcuminoid mixtures were prepared in different proportions (w/w) in according to Table 1 (considering a final concentration of 0.75 µM) based on their molecular weights. Mixture 1 (naturally extracted turmeric) was commercially obtained from PDT Pharma® (Cravinhos, São Paulo, Brazil) and its curcuminoids contents was determined by High-Performance Liquid Chromatography (HPLC) (Table S1 and Figure S1) [27].

Table 1. Mixtures of the three synthetic curcuminoids used in PDI based on quantities found through HPLC in turmeric (Mixture 1) [27], for Mixtures 2–6, a simple permutation of the percentages was proposed. The molar concentrations used in PDI for each curcuminoid are presented for a total concentration of 0.75 μM.

	CUR (%)	DMC (%)	BDMC (%)
Mixture 1	57.65% (0.43 μM)	16.35% (0.12 μM)	26.00% (0.20 μM)
Mixture 2	57.65% (0.43 μM)	26.00% (0.20 μM)	16.35% (0.12 μM)
Mixture 3	26.00% (0.20 μM)	57.65% (0.43 μM)	16.35% (0.12 μM)
Mixture 4	26.00% (0.20 μM)	16.35% (0.12 μM)	57.65% (0.43 μM)
Mixture 5	16.35% (0.12 μM)	26.00% (0.20 μM)	57.65% (0.43 μM)
Mixture 6	16.35% (0.12 μM)	57.65% (0.43 μM)	26.00% (0.20 μM)

2.2. Photobleaching and Fluorescence Emission of Curcuminoids

Individually prepared curcuminoids at 50 μM had their photobleaching spectra analyzed in a UV-vis spectrophotometer (Cary UV-vis50 spectrophotometer). Samples were illuminated with a blue LED-based device (40 mW/cm^2) for resulting fluences of 5, 10, 20, and 30 J/cm^2 as to gauge photodegradation in an expected light dose for therapy usage. Spectra were recorded in the range of 250–800 nm [28].

For fluorescence emission, curcuminoid samples were prepared at 10 μM and had their spectra obtained through a fluorimeter (Cary Eclipse Fluorescence Spectrometer), they were excited at 430 nm as absorbance spectra of all the three photosensitizers showed maxima peak near this wavelength, and fluorescence emission was recorded at the 450–750 nm range.

2.3. Photodynamic Inactivation of Staphylococcus aureus

S. aureus (ATCC 25923) bacteria inoculum was grown in 9 mL of Brain Heart Infusion (BHI) medium for 16 h and, subsequently, 1 mL of this inoculum was transferred to a new tube containing 9 mL of BHI medium for 4 h preceding the experiment, so the bacteria reached its mid-log phase. The sample was centrifuged at 3000× *g* rpm for 15 min, resuspended in phosphate-buffered saline (PBS) and diluted to adjust the bacteria inoculum to 10^8 CFU/mL using a spectrophotometer. Subsequently, 200 μL of bacteria and 200 μL of curcuminoid solution (both individual curcuminoids and their mixture) were added to a well in a 24-well plate and incubated at 37 °C for 20 min in a Bio-Oxygen Demand (BOD) incubator. The control group received no fluence from the illumination device while PDI treatment groups made use of a blue light-emitting diode (LED) (Laboratory of Technical Support, São Carlos Institute of Physics, Brazil) emitting a continuous wavelength of light emission at 462 ± 42 nm, with an average intensity of 40 mW/cm^2, which was used to illuminate the plate for PDT experiments for 4 min and 10 s to deliver a fluence of 10 J/cm^2. Energy fluences are calculated through the following formula: Fluence = Intensity × Time. Serial dilutions of the samples were performed and cultivated in BHI agar plates, following CFU counting after 24 h [29].

2.4. Statistical Analysis

The response for each experimental PDI group was tested in triplicate on three different occasions, resulting in a total sample size of nine per group (n = 9). To assess potential differences between treatment groups and after performing descriptive analysis and confirming assumptions of normality and homoscedasticity, a one-way analysis of variance (ANOVA, with Welch's correction) was performed, followed by Tukey's post hoc test. The significance level was set at 0.05 [29].

2.5. Molecular Modeling

The curcuminoid molecules were optimized using DFT [16,17], implemented in the Gaussian 16 program package [30]. Theoretical calculations were conducted employing the hybrid exchange–correlation functional with long-range correction M06-2X [31], along

with the 6-311++G(d,p) basis set. Harmonic frequency calculations were carried out to confirm that the optimized structures correspond to the energy minimum. The molecules were evaluated both in isolation and by the Solvation Model Density (SMD) continuum solvation model [31] using the solvents water (ε = 78.3553) and DMSO (ε = 46.826), which corresponds to the experimental tests. Subsequently, the molecular geometric parameters were compared using statistical tests conducted through ANOVA, followed by Tukey's post hoc test.

The electronic structures of the curcuminoid compounds were further analyzed [32]. Based on the values of the frontier molecular orbital energies, the highest occupied molecular orbital (HOMO) and the lowest unoccupied molecular orbital (LUMO), their chemical reactivity indices were calculated, including chemical hardness [33,34],

$$\eta = \frac{1}{2}\left(\frac{\partial^2 E}{\partial N^2}\right)_v = \frac{I - A}{2}, \quad (1)$$

a measure of resistance to deformation of the electron cloud during chemical processes, chemical potential [33]

$$\mu = \left(\frac{\partial E}{\partial N}\right)_v = -\frac{I + A}{2} = -\chi, \quad (2)$$

related to the charge transfer from a species with a higher chemical potential, μ_{large}, to another with a lower chemical potential, μ_{small}, and the global electrophilicity index [35],

$$\omega = \frac{\mu^2}{2\eta} \quad (3)$$

a measure of energy stabilization when the system acquires electronic charge from the environment. In Equations (1) and (2), E is the energy of the system, N is the number of particles, v is the external potential, χ is the electronegativity, $I \cong -E_{HOMO}$ is the ionization potential, and $A \cong -E_{LUMO}$ is the electron affinity. The Fukui function [36] was used to predict reactive sites favorable to radical attacks,

$$f^0 = \left[\frac{\partial \rho(\mathbf{r})}{\partial N}\right]_v^0, \quad (4)$$

where $\rho(\mathbf{r})$ is the electronic density, N is the electronic population, and v is the external potential.

To evaluate the antioxidant potential of curcuminoids, possible radicals were constructed, and their structures were optimized using the same level of theory. The results were evaluated thermodynamically to verify the curcuminoid antioxidant potential.

The effects caused by light-excited state calculations were carried out using the time-dependent density functional theory (TD-DFT) [37] at the CAM-B3LYP/6-311++G(d,p) level of theory [38]. The calculations were conducted in implicit solvent (water and DMSO), and the electronic transitions were evaluated and compared.

3. Results

3.1. Curcuminoid Photobleaching and Fluorescence Emission Spectra

The three photobleaching spectra for CUR, DMC, and BDMC are shown in Figure 2. Synthetic curcuminoids with high purity (Figures S3–S5) possess a strong characteristic peak near 420–430 nm, although BDMC showed a much broader spectrum compared to CUR and DMC (Figure 2C), indicating possible aggregation in solution. Under the same experimental conditions, the maximum absorbance recorded was 1.40 for CUR (427 nm), 1.09 for DMC (422 nm), and 0.45 for BDMC (401 nm). Upon delivering increasing amounts of fluence the samples had their absorbance decreased and slightly blue-shifted, indicating H-aggregate formation [39].

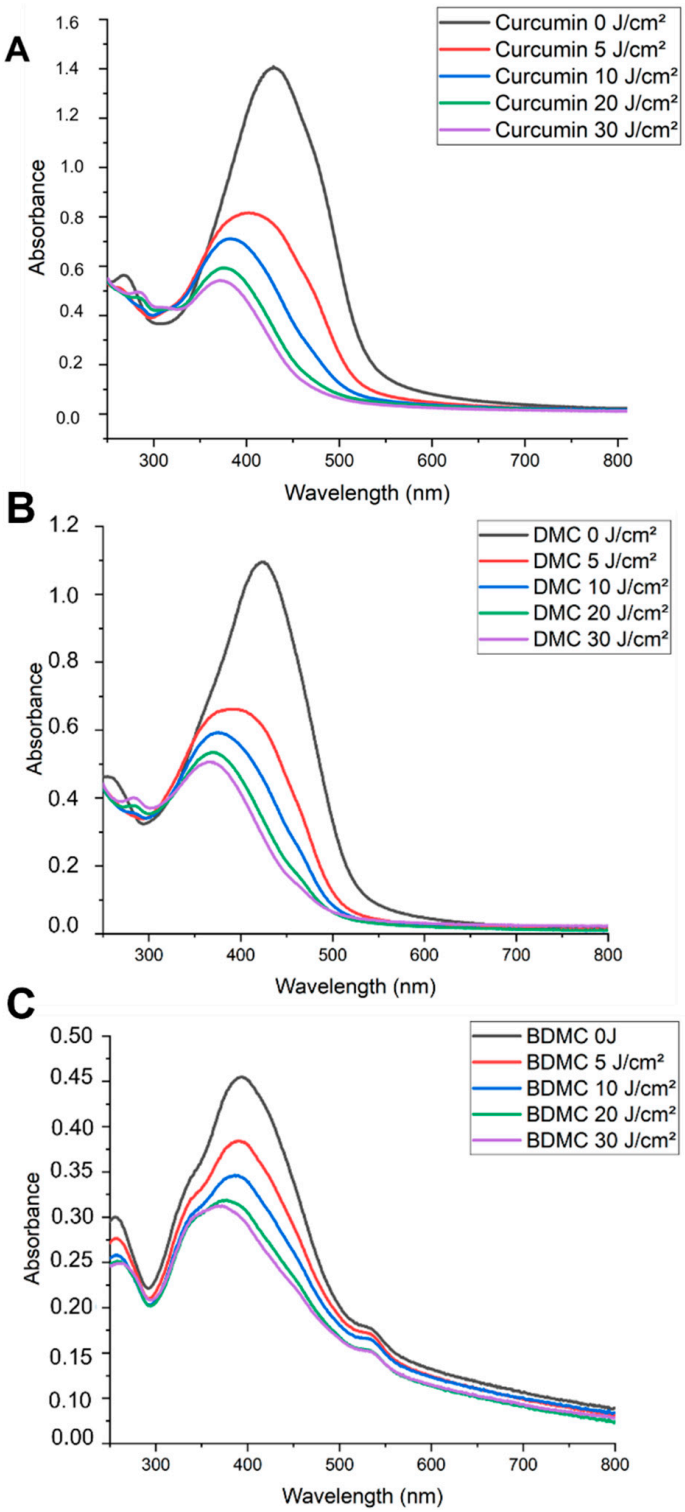

Figure 2. Photobleaching spectra of curcuminoids. (**A**) Curcumin, (**B**) DMC, and (**C**) BDMC. Curcuminoids were prepared at 50 μM in 1% DMSO solution. The spectra show the effect of increasing laser fluence (5, 10, 20, and 30 J/cm^2) on the absorbance of each curcuminoid.

Fluorescence emission spectra for the three curcuminoids are shown in Figure 3. Emissions in the broad range of 490–650 nm were observed for CUR and DMC, while BDMC showed a potent emission at 560 nm that was five times more intense than that of the other two curcuminoids.

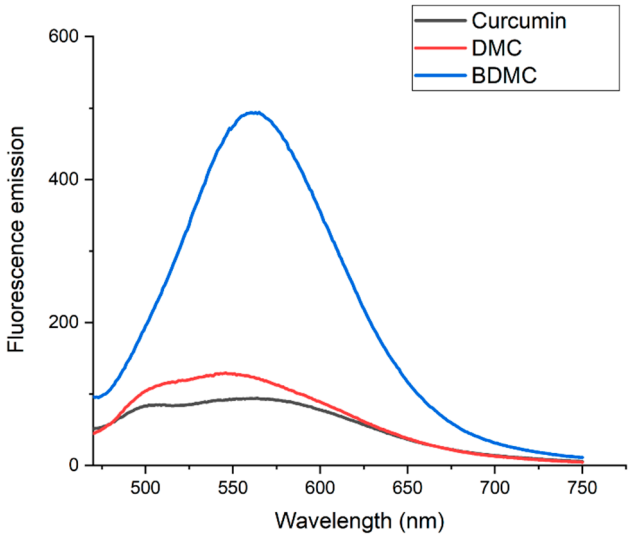

Figure 3. Fluorescence emission spectra of curcuminoids. Fluorescence emission spectra of curcumin (black line), DMC (red line), and BDMC (blue line). All curcuminoid solutions were prepared at 10 μM concentration. The excitation wavelength for all samples was set at 430 nm.

3.2. Photodynamic Inactivation of Staphylococcus aureus

Curcuminoids were first tested individually against *S. aureus*. The concentrations used were 10, 1, and 0.75 μM, and the fluence given was 10 J/cm^2. The results are shown in Figure 4.

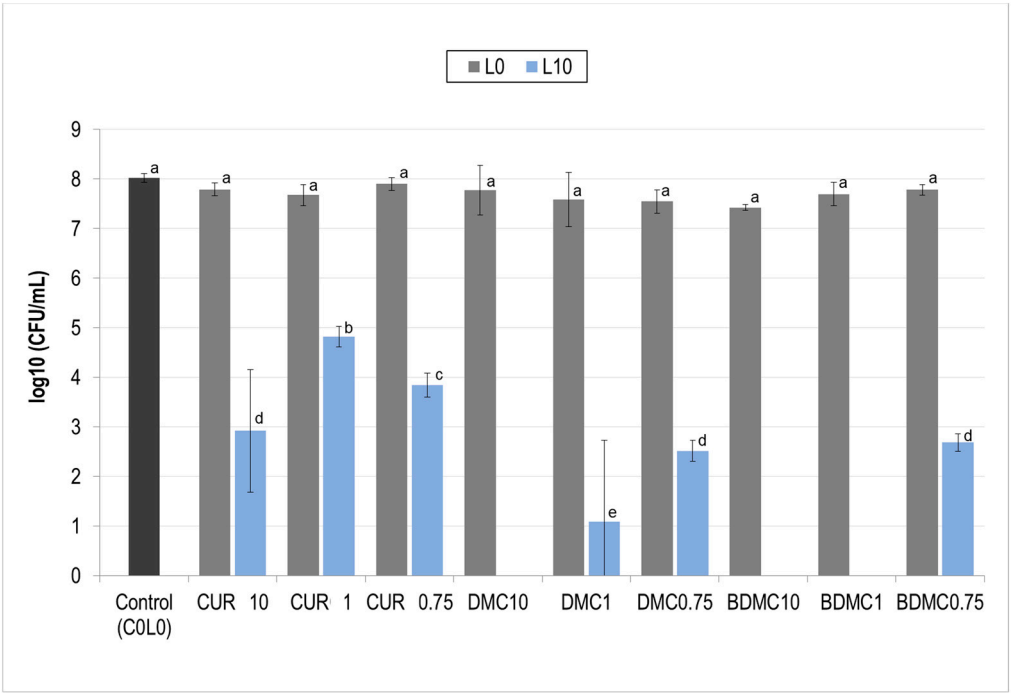

Figure 4. Photodynamic inactivation (PDI) of *Staphylococcus aureus* by curcuminoids at different concentrations. The effect of curcuminoid concentration (10, 1, and 0.75 μM) on *S. aureus* viability following photodynamic inactivation (PDI) is shown. Gray bars (L0) represent treatments without light exposure. Blue bars (L10) represent treatments with light exposure (10 J/cm^2). Different letters (a, b, c, . . .) above each bar indicate statistically significant differences between means (one-way ANOVA: $p < 0.0001$; Tukey's post hoc: $p \leq 0.039$).

In this initial screening, CUR was able to partially inactivate *S. aureus* in all concentrations while DMC and BDMC achieved complete inactivation in at 10 and 1 μM and partial inactivation with 0.75 μM. Since one of the proposed goals of this study was to test the effects of the mixture of curcuminoids and whether they were more effective than CUR by itself, the concentration of 0.75 μM was chosen in further experiments to test the mixtures.

Afterward, all mixtures (see Table 1) were prepared at 0.75 μM and tested against *S. aureus* under the same fluence conditions. Figure 5 encompasses all treatment tests and control groups in the dark (L0) and bacteria control (C0L0). Overall, an efficient decrease could be seen in all PDI groups as they showed at least a reduction of three orders of magnitude (three log) of *S. aureus*.

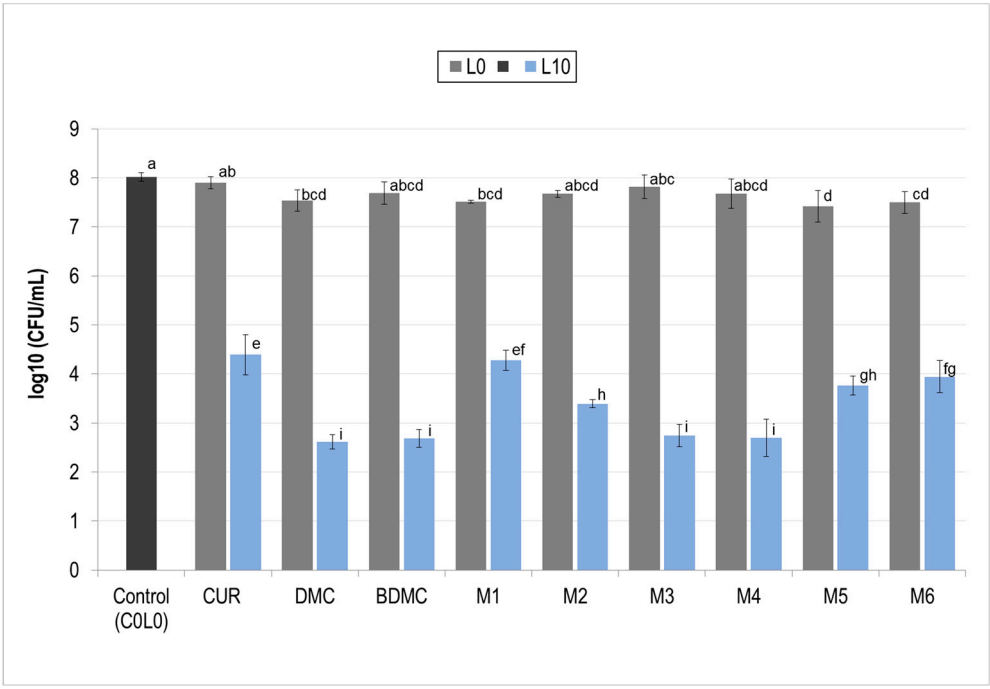

Figure 5. Photodynamic inactivation (PDI) of *Staphylococcus aureus* by individual curcuminoids and mixtures. The effectiveness of photodynamic inactivation (PDI) against *S. aureus* is shown for individual curcuminoids (CUR, DMC, and BDMC) and their mixtures (M, see Table 1). All photosensitizers were used at a concentration of 0.75 μM and irradiated with a fluence (L) of 10 J/cm^2. Gray bars represent treatments without light exposure (L0). Blue bars (L10) represent treatments with light exposure. Different letters (a, b, c, . . .) above each bar indicate statistically significant differences between means (one-way ANOVA: $p < 0.0001$; Tukey's post hoc: $p \leq 0.042$). CUR: curcumin; DMC: demethoxycurcumin; BDMC: bis-demethoxycurcumin.

These results showed that negative controls had little to no cytotoxic effects on *S. aureus* for both the individual curcuminoids as well as the proposed mixtures; the solvent used also did not reduce CFU. For all PDI treatment groups a decrease superior to 3 order of magnitude (3 logs) was achieved, curcumin (CUR L10) reduced in between 3 and 4 orders of magnitude (3.63 logs), DMC reduced bacterial count by over 5 orders of magnitude (5.41 logs), and BDMC showed similar decrease (5.34 logs). Mixture 1 was the only one to reduce *S. aureus* by less than four orders of magnitude (3.74 logs) while mixtures 2–6 all reduced bacterial count by more than four orders of magnitude (4 logs). Upon performing ANOVA, statistically, Mixtures three and four were as effective as DMC and BDMC individually and showed the biggest inactivation of bacterial cells.

3.3. Molecular Modeling

Analysis of geometric parameters showed that the curcuminoid molecules studied here are structurally similar. Statistical tests carried out by one-way ANOVA and post hoc Tukey's HSD analyses showed that neither the bond length ($p = 0.999$) nor the bond angle ($p = 0.999$) presented significantly important differences. A comparison of the structures of DMC and BDMC with curcumin indicated strong correlations in geometric parameters. However, the scatterplots in Figure 6 illustrate a roughly 2.2% increase in the C_7–C_8–O_2 angles for the curcuminoids DMC and BDMC, while the C_9–C_8–O_2 angles decreased by about 2.5%. The C_8–C_7–O_3 angle exhibited a decrease of approximately 5.2% in DMC. The boxplots in Figure 1 indicated differences in C_2–O_1 and C_2–C_3 bond lengths, which stand as outliers in the data. Similarly, the C_3–C_4–C_5 bond angles were outliers in all three compounds, as well as the C_1–C_2–C_3 and C_3'–C_2'–O_1' angles in curcumin and the C_3'–C_2'–O_1' angle in DMC.

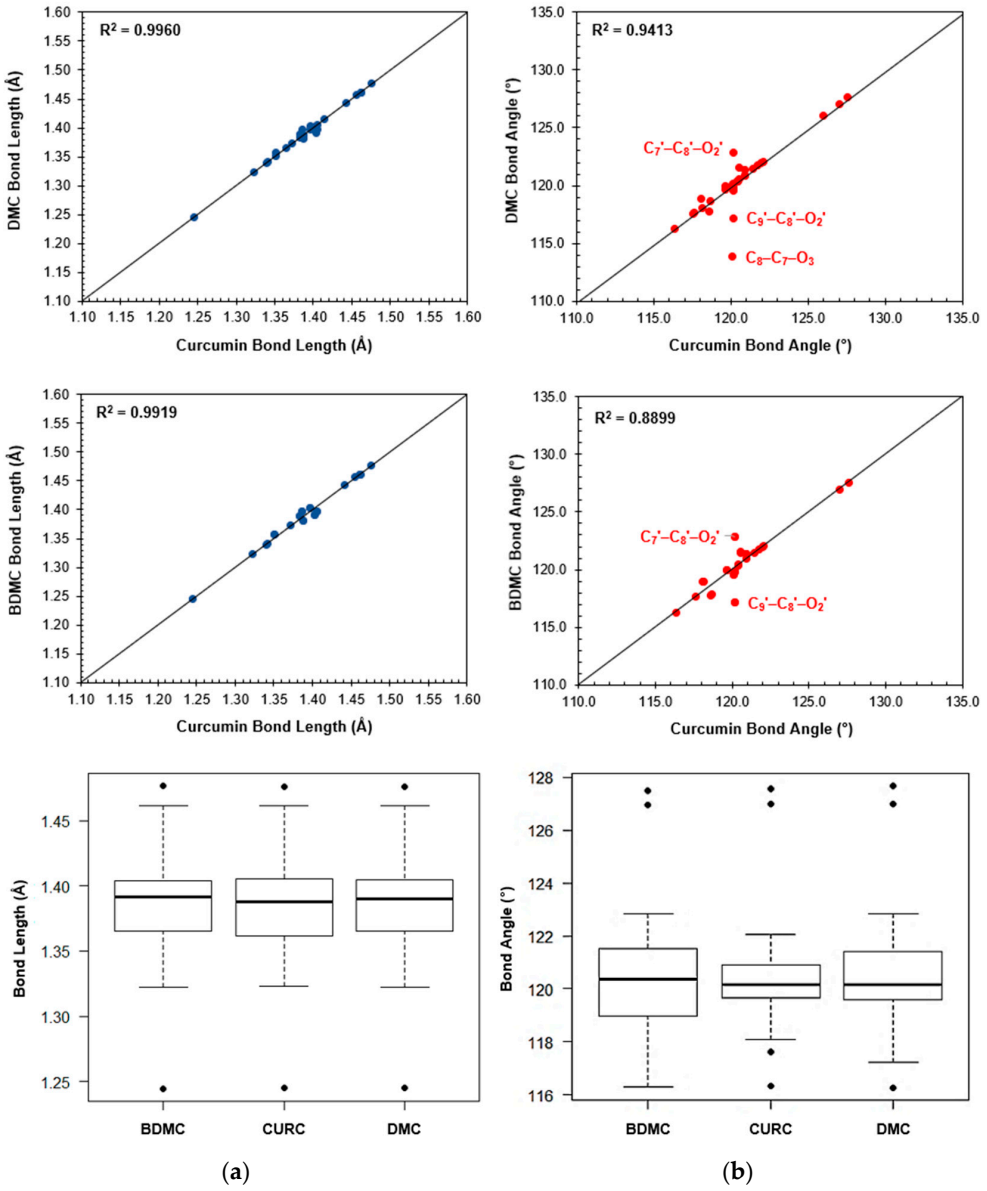

Figure 6. Comparison of bond lengths and angles between curcuminoids. This figure compares key structural features of curcuminoids using scatterplots and boxplots. Panel (**a**) shows the bond lengths between specific atoms in DMC and BDMC compared to curcumin. Panel (**b**) shows the bond angles between specific atoms in DMC and BDMC compared to CUR.

The –(CO)–CH=(COH)– system of curcuminoids exhibits keto–enol tautomerism [40–42]. It has been demonstrated that the CUR molecule in the enol form is more susceptible to electron transfer during antioxidant processes as it is electronically more reactive. For this reason, only the structures of enols were compared in this work. The isosurfaces of the frontier molecular orbitals of curcuminoid compounds are represented in Figure 7. It is possible to observe that both HOMO and LUMO are π orbitals, and their structures are similar to each other in each compound. Electronic structure calculations showed that the chemical stability of curcuminoids occurs in the order CUR < DMC < BDMC, since the values of the energy gaps increase in this order (Table 2). The lower ionization energy and high chemical potential of CUR suggest that this curcuminoid tends to transfer electrons more easily during oxidation-reduction processes. Furthermore, the lower chemical hardness indicates a greater polarizability of the electronic cloud, making it conducive to scavenging free radical processes.

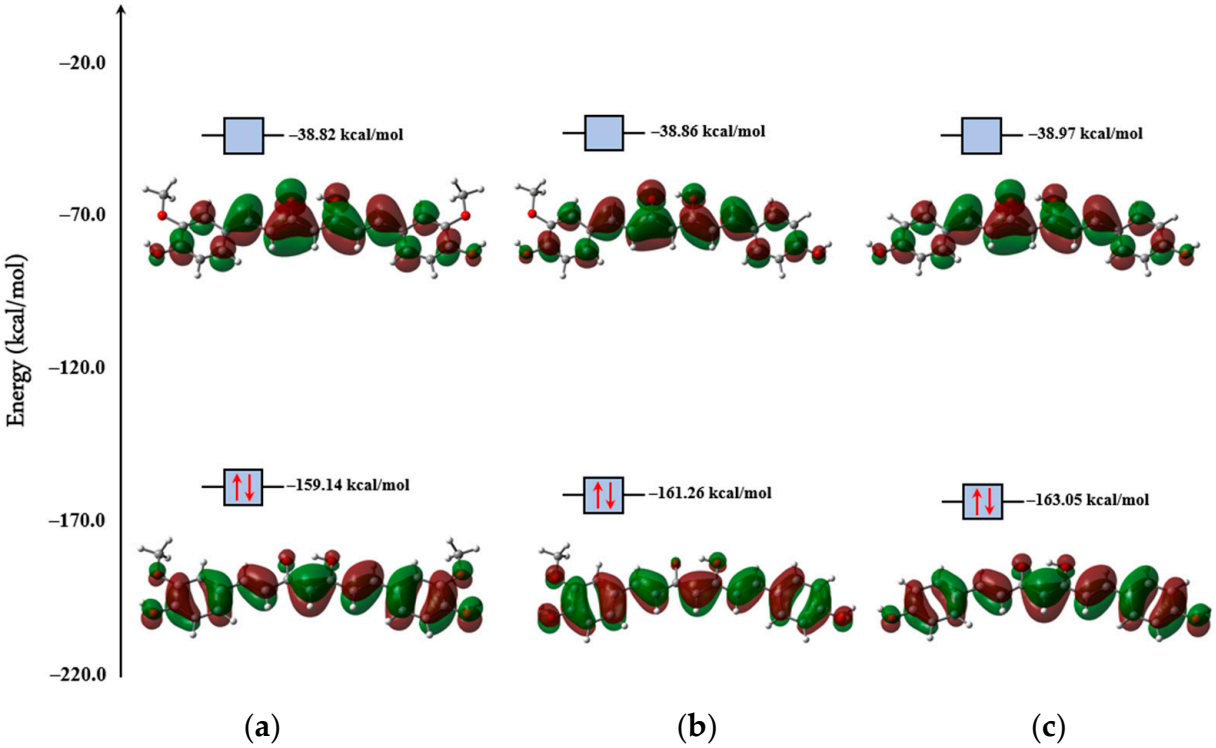

Figure 7. Electronic isodensities of the frontier molecular orbitals, HOMO (below) and LUMO (above), of the (**a**) CUR, (**b**) DMC, and (**c**) BDMC, obtained by M06-2x/6-311++G(d,p) at isovalue = 0.03. The energies of the respective orbitals are also presented.

Table 2. Reactivity indices for CUR, DMC, and BDMC obtained at M06-2X/6-311++G(d,p) level of theory. The values are in units of kcal/mol.

Descriptors	CUR	DMC	BDMC
E_{HOMO}	–159.143	–161.256	–163.050
E_{LUMO}	–38.823	–38.861	–38.974
$\Delta E_{H\text{-}L}$ *	120.320	122.396	124.076
Ionization Energy (I)	159.143	161.256	163.050
Electronic Affinity (A)	38.823	38.861	38.974
Electronegativity (χ)	98.983	100.059	101.012
Chemical potential (μ)	–98.983	–100.059	–101.012
Chemical hardness (σ)	120.320	122.396	124.076
Electrophilicity index (ω)	40.715	40.899	41.117

* $\Delta E_{H\text{-}L} = E_{LUMO} - E_{HOMO}$.

Fukui's f^0 function calculations revealed that in all three curcuminoids, free radicals can attack the phenolic O_2 (and O_2') atoms as well as the ketonic O_1 atom. An essential feature contributing to the antioxidant activity of these compounds is the presence of phenolic groups, which are present in all three compounds. Furthermore, Fukui's f^0 function indicated that C_4 (and C_4') and C_8 (and C_8') atoms are susceptible to radical attacks.

There are two known mechanisms that describe free radical scavenging: the H-atom transfer (HAT) and the one-electron transfer (ET) mechanisms. In the HAT mechanism, the antioxidant compound (AH) donates a hydrogen atom to the free radical (R·), transforming itself into a radical (A·),

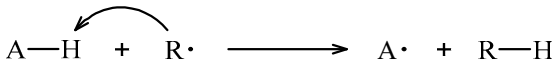

(5)

From the results of Fukui's f^0 function calculations, it is possible to observe the formation of three curcuminoid radicals by the HAT mechanism, as shown in the diagram in Figure 8. The O–H bond dissociation enthalpy calculations,

$$\mathrm{BDE(O-H)} = \left[\mathrm{H^0(A\cdot)} + \mathrm{H^0(H\cdot)}\right] - \mathrm{H^0(AH)}, \quad (6)$$

showed that the most favorable values for this mechanism occur with the removal of H atoms from phenolic groups during the free radical scavenging processes, whose values were around 87 kcal/mol. Table 3 summarizes the BDE values obtained for curcuminoids. The literature has reported that compounds with high antioxidIt ant potential have low BDE values. The average BDE values obtained for curcuminoid radicals 1 and 2 are very similar (86.77 kcal/mol for CUR, 86.79 kcal/mol for DMC, and 86.92 kcal/mol for BDMC). However, a pattern was observed for the antioxidant activity of the compounds: BDE_{CURC} < BDE_{DMC} < BDE_{BDMC}. On the other hand, the removal of the enol H atom indicated that the radical attack in this region is unfavorable since the BDE values were very high (in the order of 110 kcal/mol). This can be explained by the strong interaction existing in the system –(CO)–CH=(COH)– of the compounds, which makes it difficult for H to leave. In accordance with the quantum theory of atoms in molecules (QTAIM) [43–45] formalism, the topological parameters at the bond critical point for the O1···H–O1′ interaction in the three curcuminoids were consistent (ρ = 0.06 a.u.; ∇^2 ρ = 0.15 a.u.; h = −0.01 a.u.). According to the results of Nakanishi et al. [46,47], this interaction is identified as a very strong H-bond, whose bond energy values, calculated by the expression [48],

$$BE \approx -223.8\rho + 0.7423(\mathrm{kcal/mol}) \quad (7)$$

fall in the order of –12 kcal/mol. The aforementioned topological parameters encompass electron density (ρ), the Laplacian of ρ, ($\nabla^2\rho$), and the total electronic energy (h).

Table 3. Bond dissociation energies and ionization energy, in kcal/mol, for curcuminoid radicals obtained at M06-2X/6-311++G(d,p) level of theory.

Curcuminoid	Bond Dissociation Energy			Ionization Energy
	Radical 1	Radical 2	Radical 3	Radical 4
CUR	86.962	86.575	112.198	166.414
DMC	87.005	86.575	112.245	168.462
BDMC	87.203	86.630	112.293	170.416

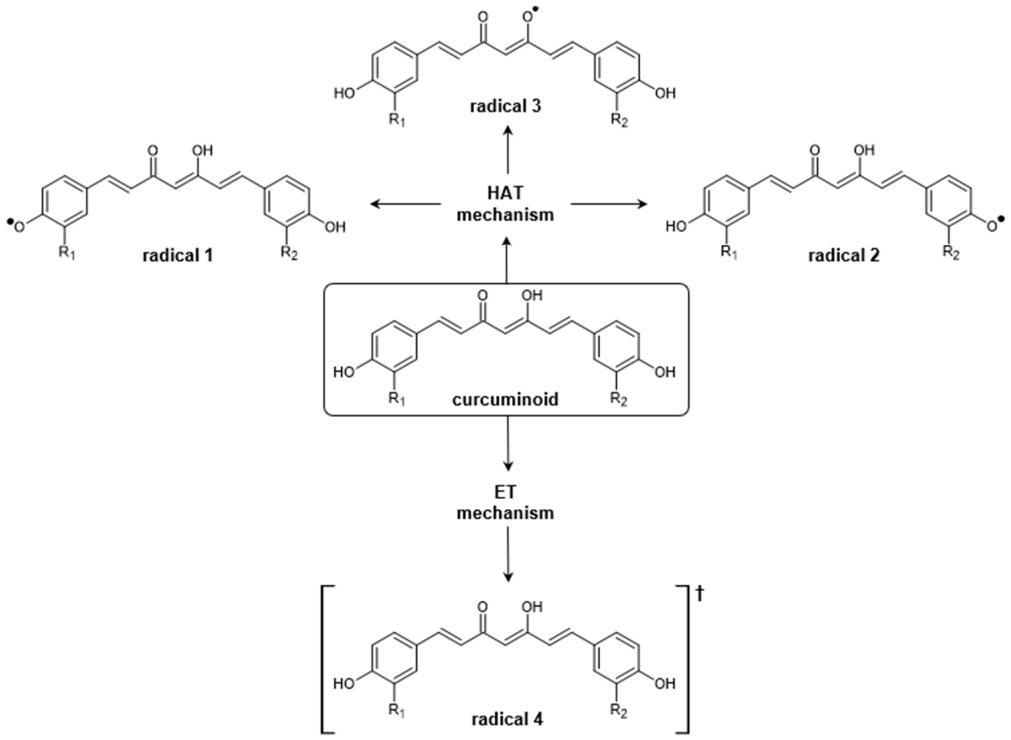

Figure 8. Diagram summarizing the H-atom transfer (HAT) and one-electron transfer (ET) mechanisms for curcuminoids. In the HAT mechanism, there is the possibility of formation of radicals 1, 2, and 3, while in the ET mechanism, only radical 4 is formed.

From the ET mechanism, the antioxidant compound (AH) transfers an electron to the free radical (R·) in order to transform itself into a radical cation (AH·$^+$), according to the chemical equation

$$AH + R\cdot \longrightarrow AH^{\cdot +} + R^{\cdot -} \quad (8)$$

Spin density calculations showed that, after electron transfer to the free radical, the unpaired electron is preferentially allocated to C1 in all curcuminoids. For the energy assessment within this mechanism, the calculation of ionization energy is commonly used

$$IE = H^0(A\cdot^+) - H^0(A - H). \quad (9)$$

Again, compounds with low IE values are potentially more antioxidant, and, in this sense, the data showed that $IE_{CUR} < IE_{DMC} < IE_{BDMC}$, corroborating the BDE results previously described (Table 3).

The spin density calculations revealed that upon hydrogen atom abstraction, to form radicals 1 and 2, the unpaired electron becomes delocalized within the aromatic rings. Natural bond orbitals (NBO) [49,50] analysis showed that hyperconjugations between donor orbitals (Lewis) and acceptor orbitals (non-Lewis) are sufficient for the stabilization of these radicals. The stability is due to the high values of stabilizing energies, estimated by the second-order perturbation formula [51],

$$E^{(2)}_{i\to j^*} = -n_\sigma \frac{\left\langle \sigma_i \middle| \hat{F} \middle| \sigma^*_j \right\rangle^2}{\varepsilon_{j^*} - \varepsilon_i} = -n_\sigma \frac{F^2_{ij}}{\varepsilon_{j^*} - \varepsilon_i}, \quad (10)$$

where $\langle \sigma | F | \sigma \rangle^2$ or F^2_{ij} is the Fock matrix element between the i, and j NBO; ε_{σ^*} is the energy of the antibonding orbital σ^*, and ε_σ is the energy of the bonding orbital σ; n_σ is the

population occupation of the σ donor orbital. The hyperconjugations and the respective $E^{(2)}_{i\to j^*}$ values are presented in Table 4. The most important factor is that they occur between the donor π orbital and the acceptor π* orbital of the aromatic ring of radicals 1 and 2. This means that the unpaired electron participates in the effect of resonance present in this region, conferring the stability of the radicals and justifying the delocalization observed in Figure 8 for this electron. Hyperconjugations between the lone pair $\eta(O_2)$ and $\eta(O_3')$ with σ* antibonding orbitals help stabilize radicals. In the case of radical 2, it is possible to observe that the –OCH_3 group helps with the stabilization of radicals of CUR through hyperconjugations carried out by the $\eta(O_3')$ orbital which are not present in DMC and BDMC. Conversely, in radical 3, the unpaired electron is equally distributed over the carbonyl oxygen atoms (O_1 and O_1') in a p orbital (notably, in DMC, the spin density is slightly higher in O_1'). In this case, weak hyperconjugations were observed in the stabilization of these radicals. They occur between bonding σ orbitals and antibonding σ^* orbitals, resulting in low $E^{(2)}_{i\to j^*}$ values. Therefore, the removal of the H· radical from the enol group of curcuminoids does not seem to be a viable path for radical formation, corroborating the results of the Fukui's $f^{\,0}$ function and the BDE data. Finally, radical 4, on the other hand, exhibits delocalization of the unpaired electron on the C_1 atom and extends toward the aliphatic region and one of the aromatic rings, albeit with low density. In this case, the radical is stabilized by hyperconjugations between bonding π and antibonding π* orbitals, whose $E^{(2)}_{i\to j^*}$ values are high. Also, the lone pairs of keto–enol oxygen atoms perform hyperconjugations with the antibonding σ* orbitals. The most notable hyperconjugation present in these radicals is $\eta_2(O_1') \to \sigma^*(C_1–C_2')$, where $E^{(2)}_{i\to j^*}$ is quite high (on the order of 35 kcal/mol) (Figure 9).

Table 4. Hyperconjugations and stabilizing energies occurring in curcuminoid radicals. The values were obtained through calculations of natural bond orbitals (NBO) at the M06-2X/6-311++G(d,p) level of theory.

	Hyperconjugation ($i\to j^*$)	**Stabilizing Energy (kcal/mol)**		
		CUR	**DMC**	**BDMC**
Radical 1	$\pi(C_6–C_7) \to \pi^*(C_5–C_{10})$	6.84	6.84	5.46
	$\pi(C_3–C_4) \to \pi^*(C_5–C_{10})$	3.74	3.74	3.41
	$\pi(C_5–C_{10}) \to \pi^*(C_6–C_7)$	17.24	17.23	18.28
	$\eta_2(O_2) \to \sigma^*(C_7–C_8)$	12.25	12.25	10.12
	$\eta_2(O_2) \to \sigma^*(C_8–C_9)$	9.83	9.83	10.15
	$\sigma(C_4–H) \to \sigma^*(C_3–H)$	3.04	3.04	2.99
Radical 2	$\pi(C_6'–C_7') \to \pi^*(C_5'–C_{10}')$	6.82	5.44	5.44
	$\pi(C_5'–C_{10}') \to \pi^*(C_5'–C_6')$	16.89	16.51	17.89
	$\eta_2(O_3') \to \pi^*(C_6'–C_7')$	16.44	-	-
	$\eta_1(O_3') \to \sigma^*(C_6'–C_7')$	4.15	-	-
	$\eta_2(O_3') \to \sigma^*(C_8'–C_9')$	9.86	-	-
	$\pi(C_1–C_2') \to \pi^*(C_3'–C_4')$	5.37	5.21	5.20
	$\pi(C_5'–C_{10}') \to \pi^*(C_3'–C_4')$	15.36	16.51	16.50
Radical 3	$\sigma(C_3–H) \to \sigma^*(C_2–O_1)$	2.14	2.15	2.15
	$\sigma(C_1–H) \to \sigma^*(C_2–O_1)$	2.03	2.03	2.03
Radical 4	$\pi(C_3'–C_4') \to \pi^*(C_1–C_2')$	14.56	16.04	16.64
	$\eta_1(O_1) \to \sigma^*(C_1–C_2)$	3.20	3.55	3.31
	$\eta_2(O_1) \to \sigma^*(C_1–C_2)$	6.52	5.61	6.58
	$\eta_1(O_1') \to \sigma^*(C_1–C_2')$	4.53	4.57	4.68
	$\eta_2(O_1') \to \sigma^*(C_1–C_2')$	36.55	38.29	39.34

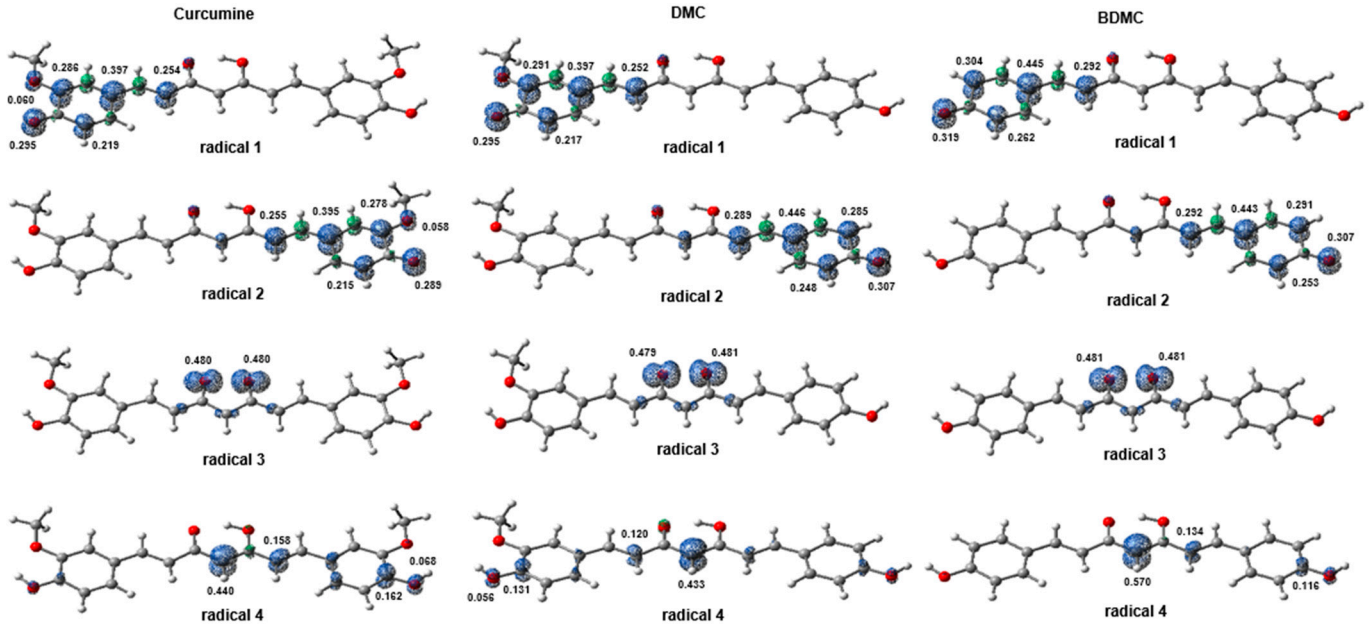

Figure 9. Isosurfaces of the spin densities (isovalue = 0.02; ρ = 0.008) of possible curcuminoid radicals formed after the elimination of free radicals, by the HAT and ET mechanisms.

In the three curcuminoid compounds, the wavelengths of maximum UV-vis absorption (λ_{max}) are located in the 300–500 nm range, as shown in Figure 10. Experimental reports indicate that these curcuminoids exhibit λ_{max} at 429 nm (CUR), 424 nm (DMC), and 419 nm (BDMC) in an ethanolic solution [52]. The λ_{max} values obtained from theoretical calculations showed slight shifts, with relative percentage errors of 5.86% observed for CUR, 5.83% for DMC, and 5.48% for BDMC. Importantly, the solvent used can influence the position of λ_{max}. Taking CUR as an example, it has been reported that the value of λ_{max} varies depending on the polarity of the solvent—from 408 nm in a non-polar solvent (CCl_4) to 430 nm in a polar solvent (DMSO)—or even if the polar solvent is protic or aprotic [53]. Consequently, in polar protic solvents like H_2O, a slight shift to higher wavelengths occurs due to strong intermolecular interactions with the solvent. Similar observations were made for the DMC and BDMC spectra, where λ_{max} values are shifted to higher wavelengths in an aqueous medium. TD-DFT calculations revealed that the λ_{max} values result from $\pi \rightarrow \pi^*$ transitions, originating from H→L excitations. Vertical excitation energies were higher in DMSO, while the oscillator strength was slightly greater in water. Chemical hardness calculations in implicit solvents indicated that curcuminoid compounds in DMSO experience orbital hardening, requiring more energy for electronic transitions. The contributions to these transitions are substantial, around 84% for CUR and DMC, and 88% for BDMC. The electronic movement during excitation occurs from the aromatic portion towards the central region of the molecules, where the chromophoric carbonyl groups are present. The $\pi \rightarrow \pi^*$ transitions arising from the S_0 to S_1 transition described previously occur in these regions, where the lone pairs of oxygen atoms and the π electrons of the C=O chromophore are responsible for the photoreactivity effects of curcuminoid compounds.

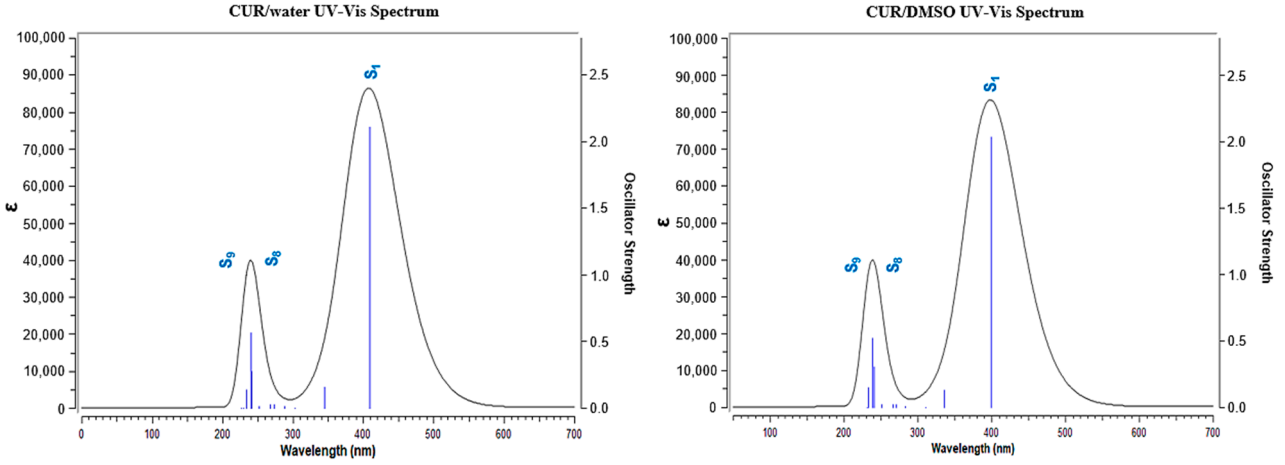

(**a**)

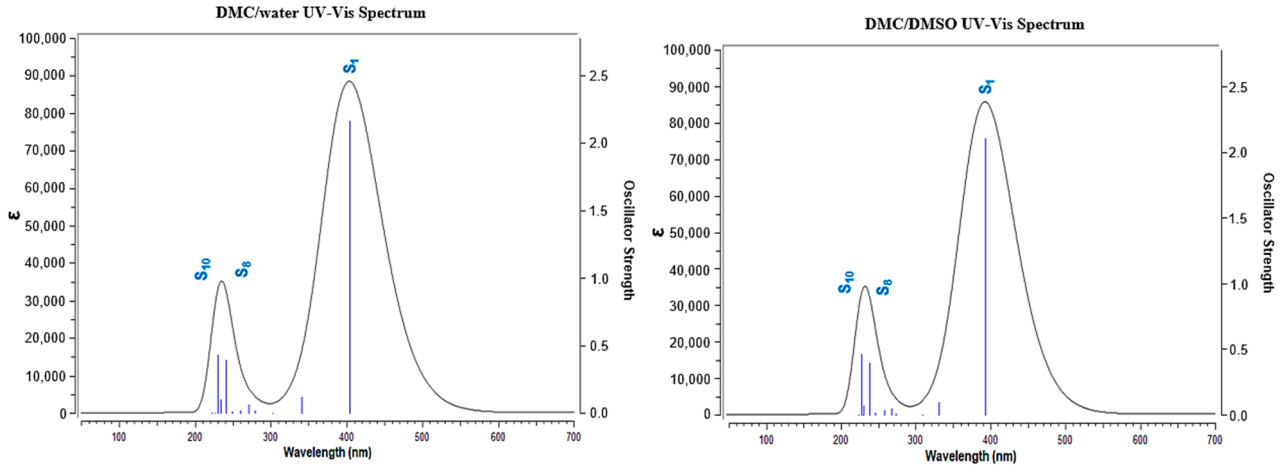

(**b**)

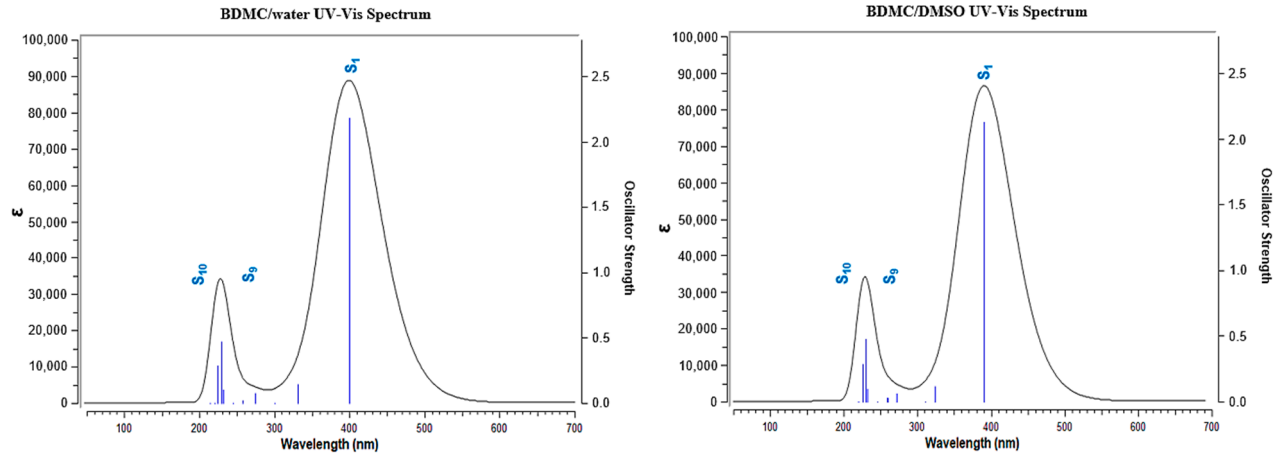

(**c**)

Figure 10. UV-vis absorption spectra of (**a**) CUR, (**b**) DMC and (**c**) BDMC. On the left are the spectra in water and on the right are the spectra in DMSO.

4. Discussion

4.1. Photobleaching and Fluorescence Emission

As previously established, this research aimed to better understand the biophysical characteristics of curcuminoids DMC and BDMC. Based on the observed photostability

of BDMC in Figure 2 and its fluorescence emission pattern in Figure 3, we propose that BDMC exhibits higher fluorescence compared to CUR and DMC. This could be attributed to BDMC's enhanced resistance to degradation under light exposure, but a more in-depth study on its fluorescence quantum yield and aggregation state is needed to confirm this hypothesis. Furthermore, the photostability of BDMC opens doors for its potential application as a diagnostic marker. This dual functionality is reminiscent of rhodamine, a common fluorescent dye used in photosensitizer development. Like rhodamine, BDMC possesses both desirable photophysical properties and chemical characteristics that make it well suited for PDT [54]. Zhang et al. [55] reported the development of a PS with fluorescence imaging capabilities that eliminates the need for a washing step during bacterial detection and treatment via image-guided photodynamic therapy. Further research with BDMC could lead to the discovery of novel and versatile applications in this field

Ali et al. [56] reported that fluorescence emission of curcuminoids varies between 548 and 575 nm, depending on CUR concentration. Their study employed fluorescence spectroscopy to compare curcuminoid levels in commercially available turmeric, exciting the entire turmeric sample at 467 nm. In contrast, our experiment specifically excited only the isolated curcuminoids. Nevertheless, the emission spectrum obtained aligns with the one reported and could indicate that the curcuminoids used in further PDI experiments have high purity.

4.2. Photodynamic Inactivation of S. aureus

As expected, treatments using only the curcuminoids were generally incapable of completely inactivating the bacteria. Although DMC and Mixtures 1, 5, and 6 differed statistically from the control group, the difference in bacterial decrease was less than 1 order of magnitude (0.5 log). PDI treatments were all able to partially inactivate the bacteria, though Mixtures 3 and 4 were the most efficient; meanwhile, isolated curcuminoids DMC and BDMC both reduced bacterial count by more than 5 orders of magnitude (5 logs), while in comparison, treatment with CUR reduced it by 3 orders of magnitude (3.63 logs).

This finding could inspire future studies on PDI, as both DMC and BDMC can be easily synthesized in large quantities [22] and in vitro results showed that they are more efficient than CUR. While the impact of combining these curcuminoids in varying ratios on overall PS efficiency remains to be elucidated, our findings suggest that individual use of DMC or BDMC might be more advantageous than a mixture. Usually, a synergistic effect can be achieved when combining two different PSs in PDT; researchers usually combine PSs to minimize the concentrations used and potentialize photodynamic effects [57,58]. As such, no synergistic effect between curcuminoids could be concluded for PDT.

As mentioned previously, not many studies investigate the potential of DMC and BDMC as PSs against bacteria, but Young et al. [59] investigated the antifungal potential of curcuminoids against Colletotrichum fungi, a genus responsible for anthracnose disease. Their in vitro studies demonstrated that all three curcuminoids (curcumin, DMC, and BDMC) significantly inhibited the growth of *C. coccodes*, *C. acutatum*, *and C. gloeosporioides* at concentrations as low as 4 μg/mL. However, in vivo tests on red pepper plants revealed that only DMC exhibited antifungal activity at 500 and 1000 μg/mL, with no phytotoxic effects observed even at concentrations exceeding 2000 μg/mL. Supporting our findings, Hung et al. [60] reported superior antibacterial efficacy of DMC and BDMC compared to CUR. Their study employed 3 μM concentrations of each curcuminoid against *Staphylococcus epidermidis* and *S. aureus*, with illumination using a 3.0 mW/cm^2 blue light source for 1 min. While CUR achieved only 14.1% elimination of bacteria, both DMC and BDMC exhibited near-complete eradication.

While research on DMC and BDMC as photosensitizers for PDI remains limited, DMC has garnered significant interest for its antitumor properties against various cancers. Studies have demonstrated its potential effectiveness against brain, ovarian, breast, lung, prostate, and skin cancers. [61]. Xin et al. [26] investigated the combination of DMC (40 μmol/L) with UV-B irradiation (60 mJ/cm^2) to enhance apoptosis in vitro against A431 cells, a model

for cutaneous squamous cell carcinoma. This approach achieved up to 35% cell death. However, Wu et al. [62] reported a higher efficacy of CUR (15 μmol/L) against the same cell line, inhibiting up to 60% of A431 cells. Notably, their study suggested that CUR's mechanism of action involved inhibiting STAT3, a key molecule in cancer cell development. These contrasting findings highlight the need for further research to determine if DMC can be a viable alternative to CUR in carcinoma treatment.

5. Conclusions

This work showed that the mixture of synthetic curcuminoids was more effective in the inactivation of *S. aureus* compared to CUR by itself; for all proposed mixtures, an equal or superior reduction was achieved. Moreover, individually, curcuminoids DMC and BDMC showed great potential as photosensitizers, as they also completely inactivated the bacteria strain with just 1 and 10 μM. Interestingly, Mixtures 3 and 4 with lower content of CUR (26%) reduced the bacterial count by higher orders of magnitude compared to mixtures with high CUR content. This property is the result of the $\pi \rightarrow \pi^*$ transition occurring in the carbonyl group that is responsible for the photoreactive effects of curcuminoids. BDMC displayed superior fluorescence emission compared to the other two curcuminoids as well as reduced photobleaching; these characteristics could allow this photosensitizer to be used in therapeutic studies and beyond the field of photodynamic therapy. The calculations showed that the molecular structures of the curcuminoid compounds are very similar. However, according to their electronic structures, there are slight differences in their kinetic stabilities and chemical reactivities. Additionally, the calculations of thermodynamic descriptors indicated that CUR and DMC have better antioxidant potential than BDMC. The radicals formed are stable only when the unpaired electron is in the aromatic regions of the curcuminoids; they do not show stability in the carbonyl groups, where electronic transitions occur in the presence of ultraviolet light.

Supplementary Materials: The following supporting information can be downloaded at https://www.mdpi.com/article/10.3390/chemistry6040035/s1, Table S1: HPLC parameters for curcuminoids analysis; Figure S1. HPLC chromatogram of natural curcumin from turmeric. Retention times: BDMC: 5474 min; DMC: 6200 min; CUR: 7002 min. Analytical standards were applied to identify the curcuminoids; Figure S2: Content of curcuminoids in natural curcumin from turmeric. CUR: 57.64%, SD = 0.044; DMC: 16.35%, SD = 0.023; BDMC: 25.99%, SD = 0.027; Figure S3: HPLC chromatogram of synthetic bis-demethoxycurcumin (BDMC); Purity: 99%; Figure S4: HPLC chromatogram of synthetic demethoxycurcumin (DMC). Purity: 96%; Figure S5: HPLC chromatogram of synthetic curcumin (CUR); Purity: 98%.

Author Contributions: Conceptualization, N.I., L.D.D. and L.N.D.; methodology, N.J.M., J.M.S., A.C.d.P. and A.S.N.A.; validation, N.J.M., N.I., J.M.S., L.D.D. and L.N.D.; formal analysis, N.J.M. and L.N.D.; investigation N.J.M.; photosensitizer's synthesis, C.C.-V. and K.T.d.O.; resources V.S.B.; data curation, N.J.M.; writing—original draft preparation, N.J.M., N.I., A.C.d.P., A.S.N.A. and L.N.D.; writing—review and editing, J.M.S., L.N.D., L.D.D., V.S.B. and K.T.d.O.; supervision, N.I. and L.N.D.; project administration, N.I., L.D.D. and V.S.B.; funding acquisition, V.S.B. All authors have read and agreed to the published version of the manuscript.

Funding: This research was funded by Fundação de Amparo à Pesquisa do Estado de São Paulo (FAPESP), grant numbers CEPOF 2013/07276-1, FAPESP 2014/50857-8, FAPESP 2020/06874-6, EMU (equipamento multiusuário) FAPESP 2021/14446-7 and the Conselho Nacional de Desenvolvimento Científico e Tecnológico (CNPq) 465360/2014-9. N. J. Melo thanks CNPq for his grant number 132139/2021-9 and Coordenação de Aperfeiçoamento de Pessoal de Nível Superior (CAPES) Finance Code 001. The authors thank Fundação de Amparo à Pesquisa do Estado de Goiás (FAPEG), Brazil (201810267001556 and Inovação, Desenvolvimento e Sustentabilidade: Estreitamento entre Universidade e Setor Produtivo no Estado de Goiás—Convênio para pesquisa, desenvolvimento e inovação—PD&I 07/2020), Coordenação de Aperfeiçoamento de Pessoal de Nível Superior, Brazil (88887.710665/2022-00). J. M. Soares thanks Coordenação de Aperfeiçoamento de Pessoal de Nível Superior (CAPES) Finance Code 001. Antônio S. N. Aguiar thanks Fundação de Amparo à Pesquisa do Estado de Goiás (FAPEG)—202110267000737. The authors thank Laboratório Teuto Brasileiro

S/A and Programa Inova Talentos (Conselho Nacional de Desenvolvimento Científico e Tecnológico (CNPq) for their financial support.

Institutional Review Board Statement: Not applicable.

Data Availability Statement: Data are contained within the article and Supplementary Materials.

Acknowledgments: The authors thank Juliana C. Barreiro for the HPLC analysis.

Conflicts of Interest: The authors declare no conflicts of interest.

References

1. Dhingra, S.; Rahman, N.A.A.; Peile, E.; Rahman, M.; Sartelli, M.; Hassali, M.A.; Islam, T.; Islam, S.; Haque, M. Microbial Resistance Movements: An Overview of Global Public Health Threats Posed by Antimicrobial Resistance, and How Best to Counter. *Front. Public Health* **2020**, *8*, 535668. [CrossRef] [PubMed]
2. Ribeiro da Cunha; Fonseca; Calado Antibiotic Discovery: Where Have We Come from, Where Do We Go? *Antibiotics* **2019**, *8*, 45. [CrossRef]
3. Aslam, B.; Wang, W.; Arshad, M.I.; Khurshid, M.; Muzammil, S.; Rasool, M.H.; Nisar, M.A.; Alvi, R.F.; Aslam, M.A.; Qamar, M.U.; et al. Antibiotic Resistance: A Rundown of a Global Crisis. *Infect. Drug Resist.* **2018**, *11*, 1645–1658. [CrossRef] [PubMed]
4. Prestinaci, F.; Pezzotti, P.; Pantosti, A. Antimicrobial Resistance: A Global Multifaceted Phenomenon. *Pathog. Glob. Health* **2015**, *109*, 309–318. [CrossRef]
5. Dadgostar, P. Antimicrobial Resistance: Implications and Costs. *Infect. Drug Resist.* **2019**, *12*, 3903–3910. [CrossRef]
6. Ghorbani, J.; Rahban, D.; Aghamiri, S.; Teymouri, A.; Bahador, A. Photosensitizers in Antibacterial Photodynamic Therapy: An Overview. *Laser Ther.* **2018**, *27*, 293–302. [CrossRef]
7. Cieplik, F.; Deng, D.; Crielaard, W.; Buchalla, W.; Hellwig, E.; Al-Ahmad, A.; Maisch, T. Antimicrobial Photodynamic Therapy—What We Know and What We Don't. *Crit. Rev. Microbiol.* **2018**, *44*, 571–589. [CrossRef]
8. Kashef, N.; Hamblin, M.R. Can Microbial Cells Develop Resistance to Oxidative Stress in Antimicrobial Photodynamic Inactivation? *Drug Resist. Updates* **2017**, *31*, 31–42. [CrossRef]
9. Dias, L.D.; Blanco, K.C.; Mfouo-Tynga, I.S.; Inada, N.M.; Bagnato, V.S. Curcumin as a Photosensitizer: From Molecular Structure to Recent Advances in Antimicrobial Photodynamic Therapy. *J. Photochem. Photobiol. C Photochem. Rev.* **2020**, *45*, 100384. [CrossRef]
10. Robertson, C.A.; Evans, D.H.; Abrahamse, H. Photodynamic Therapy (PDT): A Short Review on Cellular Mechanisms and Cancer Research Applications for PDT. *J. Photochem. Photobiol. B* **2009**, *96*, 1–8. [CrossRef]
11. Chen, D.; Xu, Q.; Wang, W.; Shao, J.; Huang, W.; Dong, X. Type I Photosensitizers Revitalizing Photodynamic Oncotherapy. *Small* **2021**, *17*, 2006742. [CrossRef] [PubMed]
12. Lucky, S.S.; Soo, K.C.; Zhang, Y. Nanoparticles in Photodynamic Therapy. *Chem. Rev.* **2015**, *115*, 1990–2042. [CrossRef] [PubMed]
13. Szabo, A.; Ostlund, N.S. *Modern Quantum Chemistry: Introduction to Advanced Electronic Structure Theory*, 1st ed.; McGraw-Hill: New York, NY, USA, 1996.
14. Parr, R.G.; Yang, W. *Density-Functional Theory of Atoms and Molecules*; Oxford University Press: New York, NY, USA, 1995; ISBN 9780195092769.
15. Thiel, W. Semiempirical Quantum–Chemical Methods. *WIREs Comput. Mol. Sci.* **2014**, *4*, 145–157. [CrossRef]
16. Hohenberg, P.; Kohn, W. Inhomogeneous Electron Gas. *Phys. Rev.* **1964**, *136*, B864. [CrossRef]
17. Kohn, W.; Sham, L.J. Self-Consistent Equations Including Exchange and Correlation Effects. *Phys. Rev.* **1965**, *140*, A1133–A1138. [CrossRef]
18. Sholl, D.S.; Steckel, J.A. *Density Functional Theory: A Practical Introduction*; John Wiley & Sons: Hoboken, NJ, USA, 2022; ISBN 9780470373170.
19. Sueth-Santiago, V.; Mendes-Silva, G.P.; Decoté-Ricardo, D.; de Lima, M.E.F. Curcumin, the Golden Powder from Turmeric: Insights into Chemical and Biological Activities. *Quim. Nova* **2015**, *38*, 538–552. [CrossRef]
20. Priyadarsini, K. The Chemistry of Curcumin: From Extraction to Therapeutic Agent. *Molecules* **2014**, *19*, 20091–20112. [CrossRef] [PubMed]
21. Chintakovid, N.; Tisarum, R.; Samphumphuang, T.; Sotesaritkul, T.; Cha-Um, S. Evaluation of Curcuminoids, Physiological Adaptation, and Growth of Curcuma Longa under Water Deficit and Controlled Temperature. *Protoplasma* **2022**, *259*, 301–315. [CrossRef]
22. Carmona-Vargas, C.C.; de Alves, L.C.; Brocksom, T.J.; de Oliveira, K.T. Combining Batch and Continuous Flow Setups in the End-to-End Synthesis of Naturally Occurring Curcuminoids. *React. Chem. Eng.* **2017**, *2*, 366–374. [CrossRef]
23. Hatamipour, M.; Ramezani, M.; Tabassi, S.A.S.; Johnston, T.P.; Ramezani, M.; Sahebkar, A. Demethoxycurcumin: A Naturally Occurring Curcumin Analogue with Antitumor Properties. *J. Cell Physiol.* **2018**, *233*, 9247–9260. [CrossRef]
24. Lin, H.-Y.; Lin, J.-N.; Ma, J.-W.; Yang, N.-S.; Ho, C.-T.; Kuo, S.-C.; Way, T.-D. Demethoxycurcumin Induces Autophagic and Apoptotic Responses on Breast Cancer Cells in Photodynamic Therapy. *J. Funct. Foods* **2015**, *12*, 439–449. [CrossRef]
25. Wu, Y.; Zhang, P.; Yang, H.; Ge, Y.; Xin, Y. Effects of Demethoxycurcumin on the Viability and Apoptosis of Skin Cancer Cells. *Mol. Med. Rep.* **2017**, *16*, 539–546. [CrossRef] [PubMed]

26. Xin, Y.; Huang, Q.; Zhang, P.; Guo, W.W.; Zhang, L.Z.; Jiang, G. Demethoxycurcumin in Combination with Ultraviolet Radiation B Induces Apoptosis through the Mitochondrial Pathway and Caspase Activation in A431 and HaCaT Cells. *Tumor Biol.* **2017**, *39*, 101042831770621. [CrossRef] [PubMed]
27. Da Silva, A.P. Novas Estratégias Para o Diagnóstico de Onicomicose e Tratamento Por Terapia Fotodinâmica. Ph.D. Thesis, Universidade de São Paulo, São Carlos, Brazil, 2017.
28. Dias, L.D.; Corrêa, T.Q.; Bagnato, V.S. Cooperative and Competitive Antimicrobial Photodynamic Effects Induced by a Combination of Methylene Blue and Curcumin. *Laser Phys. Lett.* **2021**, *18*, 075601. [CrossRef]
29. de Melo, N.J.; Tovar, J.S.D.; Dovigo, L.N.; Dias, L.D.; Bagnato, V.S.; Inada, N.M. Natural versus Synthetic Curcuminoids as Photosensitizers: Photobleaching and Antimicrobial Photodynamic Therapy Evaluation. *Photodiagn. Photodyn. Ther.* **2023**, *42*, 103495. [CrossRef] [PubMed]
30. Frisch, G.W.M.J.; Trucks, H.B.; Schlegel, G.E.; Scuseria, M.A.; Robb, J.R.; Cheeseman, G.; Scalmani, V.; Barone, G.A.; Petersson, H.; Nakatsuji, X. Peralta, Gaussian 16, Revision C.01. Wallingford CT. 2016. Available online: https://gaussian.com/citation/ (accessed on 14 July 2024).
31. Zhao, Y.; Truhlar, D.G. The M06 Suite of Density Functionals for Main Group Thermochemistry, Thermochemical Kinetics, Noncovalent Interactions, Excited States, and Transition Elements: Two New Functionals and Systematic Testing of Four M06-Class Functionals and 12 Other Functionals. *Theor. Chem. Acc.* **2008**, *120*, 215–241. [CrossRef]
32. Zhang, G.; Musgrave, C.B. Comparison of DFT Methods for Molecular Orbital Eigenvalue Calculations. *J. Phys. Chem. A* **2007**, *111*, 1554–1561. [CrossRef] [PubMed]
33. Pearson, R.G. The Electronic Chemical Potential and Chemical Hardness. *J. Mol. Struct. THEOCHEM* **1992**, *255*, 261–270. [CrossRef]
34. Makov, G. Chemical Hardness in Density Functional Theory. *J. Phys. Chem.* **1995**, *99*, 9337–9339. [CrossRef]
35. Parr, R.G.; Szentpály, L.V.; Liu, S. Electrophilicity Index. *J. Am. Chem. Soc.* **1999**, *121*, 1922–1924. [CrossRef]
36. Fukui, K. Role of Frontier Orbitals in Chemical Reactions. *Science* **1982**, *218*, 747–754. [CrossRef] [PubMed]
37. Bauernschmitt, R.; Ahlrichs, R. Treatment of Electronic Excitations within the Adiabatic Approximation of Time Dependent Density Functional Theory. *Chem. Phys. Lett.* **1996**, *256*, 454–464. [CrossRef]
38. Yanai, T.; Tew, D.P.; Handy, N.C. A New Hybrid Exchange–Correlation Functional Using the Coulomb-Attenuating Method (CAM-B3LYP). *Chem. Phys. Lett.* **2004**, *393*, 51–57. [CrossRef]
39. Ghosh, S.; Li, X.; Stepanenko, V.; Würthner, F. Control of H- and J-Type π Stacking by Peripheral Alkyl Chains and Self-Sorting Phenomena in Perylene Bisimide Homo- and Heteroaggregates. *Chem. A Eur. J.* **2008**, *14*, 11343–11357. [CrossRef] [PubMed]
40. Sharma, R.A.; Gescher, A.J.; Steward, W.P. Curcumin: The Story so Far. *Eur. J. Cancer* **2005**, *41*, 1955–1968. [CrossRef]
41. Anand, P.; Thomas, S.G.; Kunnumakkara, A.B.; Sundaram, C.; Harikumar, K.B.; Sung, B.; Tharakan, S.T.; Misra, K.; Priyadarsini, I.K.; Rajasekharan, K.N.; et al. Biological Activities of Curcumin and Its Analogues (Congeners) Made by Man and Mother Nature. *Biochem. Pharmacol.* **2008**, *76*, 1590–1611. [CrossRef] [PubMed]
42. Dias, L.D.; Aguiar, A.S.N.; de Melo, N.J.; Inada, N.M.; Borges, L.L.; de Aquino, G.L.B.; Camargo, A.J.; Bagnato, V.S.; Napolitano, H.B. Structural Basis of Antibacterial Photodynamic Action of Curcumin against *S. aureus*. *Photodiagn. Photodyn. Ther.* **2023**, *43*, 103654. [CrossRef]
43. Bader, R.F.W.; Nguyen-Dang, T.T.; Tal, Y. A Topological Theory of Molecular Structure. *Rep. Progress. Phys.* **1981**, *44*, 893–948. [CrossRef]
44. Bader, R.F.W.; Essén, H. The Characterization of Atomic Interactions. *J. Chem. Phys.* **1984**, *80*, 1943–1960. [CrossRef]
45. Bader, R.F.W.; MacDougall, P.J. Toward a Theory of Chemical Reactivity Based on the Charge Density. *J. Am. Chem. Soc.* **1985**, *107*, 6788–6795. [CrossRef]
46. Nakanishi, W.; Hayashi, S.; Narahara, K. Atoms-in-Molecules Dual Parameter Analysis of Weak to Strong Interactions: Behaviors of Electronic Energy Densities versus Laplacian of Electron Densities at Bond Critical Points. *J. Phys. Chem. A* **2008**, *112*, 13593–13599. [CrossRef]
47. Nakanishi, W.; Hayashi, S.; Narahara, K. Polar Coordinate Representation of $H_b(r_c)$ versus $(\hbar^2/8m) \bigtriangledown^2 \rho_b(r_c)$ at BCP in AIM Analysis: Classification and Evaluation of Weak to Strong Interactions. *J. Phys. Chem. A* **2009**, *113*, 10050. [CrossRef]
48. Emamian, S.; Lu, T.; Kruse, H.; Emamian, H. Exploring Nature and Predicting Strength of Hydrogen Bonds: A Correlation Analysis Between Atoms-in-Molecules Descriptors, Binding Energies, and Energy Components of Symmetry-Adapted Perturbation Theory. *J. Comput. Chem.* **2019**, *40*, 2868–2881. [CrossRef]
49. Weinhold, F.; Landis, C.R. *Discovering Chemistry with Natural Bond Orbitals*; Wiley: Hoboken, NJ, USA, 2012; ISBN 9781118119969.
50. Weinhold, F.; Landis, C.R. Natural Bond Orbitals and Extensions of Localized Bonding Concepts. *Chem. Educ. Res. Pract.* **2001**, *2*, 91–104. [CrossRef]
51. Alabugin, I.V.; Gilmore, K.M.; Peterson, P.W. Hyperconjugation. *WIREs Comput. Mol. Sci.* **2011**, *1*, 109–141. [CrossRef]
52. Péret-Almeida, L.; Cherubino, A.P.F.; Alves, R.J.; Dufossé, L.; Glória, M.B.A. Separation and Determination of the Physico-Chemical Characteristics of Curcumin, Demethoxycurcumin and Bisdemethoxycurcumin. *Food Res. Int.* **2005**, *38*, 1039–1044. [CrossRef]
53. Jasim, F.; Ali, F. Measurements of Some Spectrophotometric Parameters of Curcumin in 12 Polar and Nonpolar Organic Solvents. *Microchem. J.* **1989**, *39*, 156–159. [CrossRef]

54. Li, L.; Chen, Y.; Chen, W.; Tan, Y.; Chen, H.; Yin, J. Photodynamic Therapy Based on Organic Small Molecular Fluorescent Dyes. *Chin. Chem. Lett.* **2019**, *30*, 1689–1703. [CrossRef]
55. Zhang, Y.; Zhao, X.; Li, Y.; Wang, X.; Wang, Q.; Lu, H.; Zhu, L. A Fluorescent Photosensitizer with Far Red/near-Infrared Aggregation-Induced Emission for Imaging and Photodynamic Killing of Bacteria. *Dye. Pigment.* **2019**, *165*, 53–57. [CrossRef]
56. Ali, Z.; Saleem, M.; Atta, B.M.; Khan, S.S.; Hammad, G. Determination of Curcuminoid Content in Turmeric Using Fluorescence Spectroscopy. *Spectrochim. Acta A Mol. Biomol. Spectrosc.* **2019**, *213*, 192–198. [CrossRef]
57. Tosato, M.G.; Schilardi, P.; Lorenzo de Mele, M.F.; Thomas, A.H.; Lorente, C.; Miñán, A. Synergistic Effect of Carboxypterin and Methylene Blue Applied to Antimicrobial Photodynamic Therapy against Mature Biofilm of *Klebsiella pneumoniae*. *Heliyon* **2020**, *6*, e03522. [CrossRef]
58. Pourhajibagher, M.; Plotino, G.; Chiniforush, N.; Bahador, A. Dual Wavelength Irradiation Antimicrobial Photodynamic Therapy Using Indocyanine Green and Metformin Doped with Nano-Curcumin as an Efficient Adjunctive Endodontic Treatment Modality. *Photodiagn. Photodyn. Ther.* **2020**, *29*, 101628. [CrossRef]
59. Cho, J.Y.; Choi, G.J.; Lee, S.W.; Jang, K.S.; Lim, H.K.; Lim, C.H.; Lee, S.O.; Cho, K.Y.; Kim, J.C. Antifungal Activity against Colletotrichum spp. of Curcuminoids Isolated from Curcuma longa L. Rhizomes. *J. Microbiol. Biotechnol.* **2006**, *16*, 280–285.
60. Hung, S.-J.; Hong, Y.-A.; Lin, K.-Y.; Hua, Y.-W.; Kuo, C.-J.; Hu, A.; Shih, T.-L.; Chen, H.-P. Efficient Photodynamic Killing of Gram-Positive Bacteria by Synthetic Curcuminoids. *Int. J. Mol. Sci.* **2020**, *21*, 9024. [CrossRef]
61. Hatamipour, M.; Ramezani, M.; Tabassi, S.A.S.; Johnston, T.P.; Sahebkar, A. Demethoxycurcumin: A Naturally Occurring Curcumin Analogue for Treating Non-cancerous Diseases. *J. Cell Physiol.* **2019**, *234*, 19320–19330. [CrossRef]
62. Wu, J.; Lu, W.-Y.; Cui, L.-L. Inhibitory Effect of Curcumin on Invasion of Skin Squamous Cell Carcinoma A431 Cells. *Asian Pac. J. Cancer Prev.* **2015**, *16*, 2813–2818. [CrossRef]